AIP Applied Physics Letters

Effects of the oxygen vacancy concentration in InGaZnO-based resistance random access memory

Moon-Seok Kim, Young Hwan Hwang, Sungho Kim, Zheng Guo, Dong-Il Moon et al.

Citation: Appl. Phys. Lett. **101**, 243503 (2012); doi: 10.1063/1.4770073
View online: http://dx.doi.org/10.1063/1.4770073
View Table of Contents: http://apl.aip.org/resource/1/APPLAB/v101/i24
Published by the American Institute of Physics.

Related Articles

Influence of molybdenum doping on the switching characteristic in silicon oxide-based resistive switching memory
Appl. Phys. Lett. 102, 043508 (2013)

Metal-oxide-semiconductor diodes containing C60 fullerenes for non-volatile memory applications
J. Appl. Phys. 113, 044520 (2013)

Graphene nanoribbon based negative resistance device for ultra-low voltage digital logic applications
Appl. Phys. Lett. 102, 043114 (2013)

Demonstration and modeling of multi-bit resistance random access memory
Appl. Phys. Lett. 102, 043502 (2013)

Role of oxygen vacancies in TiO2-based resistive switches
J. Appl. Phys. 113, 033707 (2013)

Additional information on Appl. Phys. Lett.

Journal Homepage: http://apl.aip.org/
Journal Information: http://apl.aip.org/about/about_the_journal
Top downloads: http://apl.aip.org/features/most_downloaded
Information for Authors: http://apl.aip.org/authors

ADVERTISEMENT

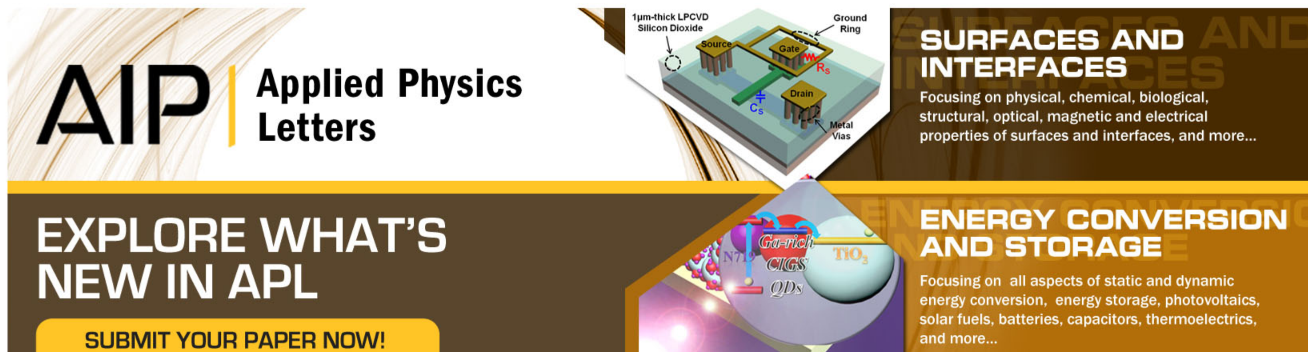

Downloaded 03 Feb 2013 to 143.248.118.122. Redistribution subject to AIP license or copyright; see http://apl.aip.org/about/rights_and_permissions

Effects of the oxygen vacancy concentration in InGaZnO-based resistance random access memory

Moon-Seok Kim,[1] Young Hwan Hwang,[2] Sungho Kim,[1] Zheng Guo,[1] Dong-Il Moon,[1] Ji-Min Choi,[1] Myeong-Lok Seol,[1] Byeong-Soo Bae,[2] and Yang-Kyu Choi[1,a)]
[1]Department of Electrical Engineering, KAIST, 291 Daehak-ro, Yuseong-gu, Daejeon 305-701, South Korea
[2]Department of Materials Science and Engineering, KAIST, 291 Daehak-ro, Yuseong-gu, Daejeon 305-701, South Korea

(Received 13 August 2012; accepted 21 November 2012; published online 10 December 2012)

Resistance random access memory (RRAM) composed of stacked aluminum (Al)/InGaZnO(IGZO)/Al is investigated with different gallium concentrations. The stoichiometric ratio (x) of gallium in the $InGa_xZnO$ is varied from 0 to 4 for intentional control of the concentration of the oxygen vacancies (V_O), which influences the electrical characteristics of the RRAM. No Ga in the IGZO ($x = 0$) significantly increases the value of V_O and leads to a breakdown of the IGZO. In contrast, a high Ga concentration ($x = 4$) suppresses the generation of V_O; hence, resistive switching is disabled. The optimal value of x is 2. Accordingly, enduring RRAM characteristics are achieved. © *2012 American Institute of Physics*. [http://dx.doi.org/10.1063/1.4770073]

InGaZnO (IGZO) has attracted a great deal of attention in recent years as a channel material for use in thin film transistors (TFTs). IGZO has several advantages when used as an active layer in TFTs, including transparency and high mobility, even in an amorphous state, which are important requirements for flat-panel display applications.[1] The electrical characteristics of IGZO TFTs mainly depend on the concentrations of indium and gallium.[2] It is well known that an increased concentration of indium enhances the mobility of TFTs and that the addition of gallium suppresses the generation of oxygen vacancies (V_O).[3,4]

Meanwhile, resistive random access memory (RRAM) is a nonvolatile type of memory that utilizes the resistive switching (RS) behavior between a high-resistance state (HRS) and a low-resistance state (LRS) for the construction of a bi-stable state. RRAM has attracted considerable attention as a transparent and flexible memory device because of its promising electrical characteristics, such as low power consumption and high speed.[5–8] Amorphous IGZO (a-IGZO) is a potential candidate for RRAM devices due to the nature of its transparency and its low-temperature processing. The electrical characteristics of IGZO have been investigated with respect to the stoichiometric ratio (composition ratio).[9,10] One of the advantages of IGZO is that its electrical properties can easily be modulated by controlling the stoichiometric ratio of indium and gallium. In particular, the increased concentration of gallium in IGZO suppresses the generation of V_O, which plays a role in carrier transport. This phenomenon was applied to IGZO-TFT devices to decrease the off-state current, which is crucial for minimizing the power consumption.[11] Therefore, if the mechanism of bipolar resistive switching (BRS) strongly relies on the concentration of V_O, it is inferred that deliberately controlling the oxygen vacancy concentration may be suitable for IGZO-based RRAM.[12] It was experimentally demonstrated that IGZO shows RS characteristics.[13,14] Specifically, the RS characteristics based on oxygen ion migration in a-IGZO were utilized for a synaptic device with inherent learning and memory functions.[15] However, controllable resistive switching characteristics, which are affected by the concentration of V_O, have not been comprehensively investigated. Thus, it is timely to study how the oxygen vacancy concentration in the IGZO-based RRAM influences the RS characteristics.

In this study, an adjustment of the gallium concentration is adopted to modulate the concentration of V_O by controlling the activation energy for annihilation of oxygen vacancies.[16] It should be noted that the purpose of controlling the gallium concentration is to study how an intentionally engineered oxygen vacancy concentration affects the characteristics of IGZO-based RRAM. The implemented RRAM comprises three layers: Al (top electrode), IGZO (resistive switching material), and Al (bottom electrode). The stoichiometric ratio (x) of gallium in the composite of In:Ga:Zn $= 1{:}x{:}1$ is varied from 0 to 4 to control the concentration of V_O because this concentration influences the RS characteristics. The electrical properties of the fabricated RRAM are analyzed with different values of x. The oxygen concentration dependency is also analyzed with the aid of electron energy-loss spectroscopy (EELS).

An Al layer thickness of 50 nm was used as the top electrode (TE) and the bottom electrode (BE). The Al was deposited by a thermal evaporator. Conventional photolithography and chemical etching were employed to pattern the electrodes. An IGZO thin film was deposited by a sol-gel method. Indium(III) nitrate hydrate, gallium(III) nitrate hydrate, and zinc nitrate hexahydrate were used as precursors. The molar concentration of the indium and zinc precursors was fixed at 0.1 M. The molar ratio of the gallium precursors was varied from 0 to 4 in a composite of In:Ga:Zn $= 1{:}x{:}1$. All precursors were dissolved in a 10 ml volume of 2-methoxyethanol. Spin coating was performed at 5000 rpm for 30 s. The coated substrates were annealed at 370 °C for 2 h in air to evaporate out the solvent. These IGZO samples are known to be in an amorphous state when annealed at 370 °C.[17] The inset of

[a)]Author to whom correspondence should be addressed. Electronic mail: ykchoi@ee.kaist.ac.kr.

 © 2012 American Institute of Physics

Downloaded 03 Feb 2013 to 143.248.118.122. Redistribution subject to AIP license or copyright; see http://apl.aip.org/about/rights_and_permissions

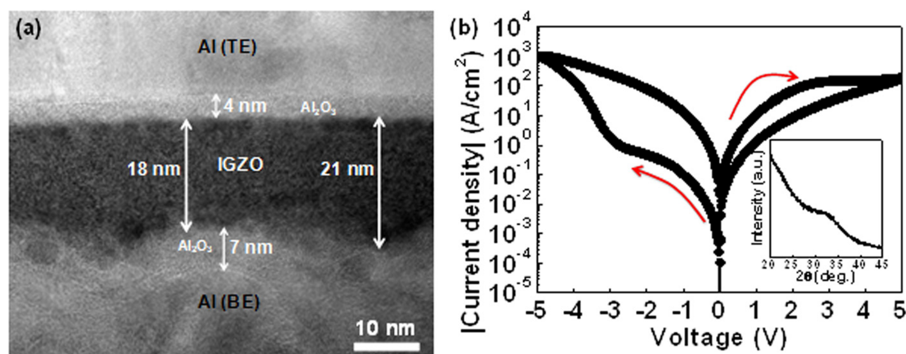

FIG. 1. (a) A cross-sectional TEM image of a stacked Al/a-IGZO/Al structure in In:Ga:Zn = 1:2:1. (b) Typical current density-voltage (*J-V*) curve of RRAM consisting of an Al/a-IGZO/Al device with In:Ga:Zn = 1:2:1 during a bipolar voltage sweep. Arrows indicate the direction of the voltage sweep. The inset represents XRD data for the deposited IGZO annealed at 370 °C.

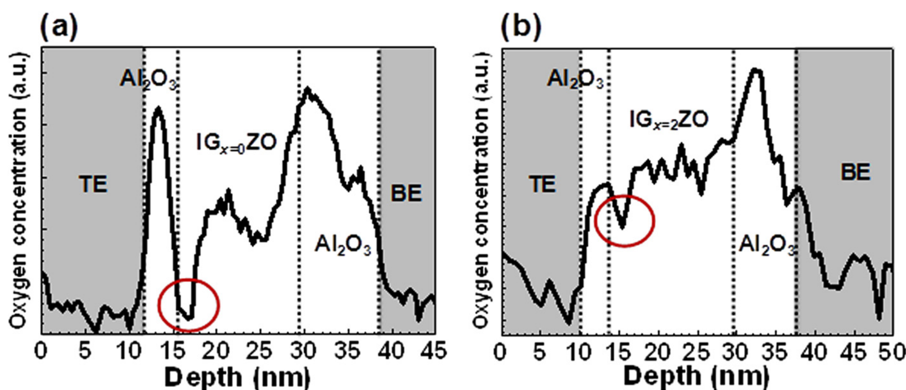

FIG. 2. The oxygen-concentration profile based on an EELS analysis with respect to the depth for (a) In:Ga:Zn = 1:0:1 and (b) In:Ga:Zn = 1:2:1.

Fig. 1(b) verifies that the deposited IGZO is in an amorphous state according to an X-ray diffraction (XRD) analysis. Fig. 1(a) shows a cross-sectional transmission electron microscopy (TEM) image of the fabricated Al/a-IGZO/Al device. Regardless of the gallium concentration, the thickness of Al_2O_3 between the top electrode and IGZO is approximately 4 nm, whereas that between the bottom electrode and IGZO is approximately 8 nm. The thickness of IGZO at $x = 2$ is approximately 18 to 21 nm. It was reported that the modulation of the gallium concentration did not make a significant difference in the IGZO thicknesses.[18] The roughly estimated average thickness of IGZO is 20 nm, irrespective of the gallium concentration.

Figs. 2(a) and 2(b) show the oxygen concentration as analyzed by EELS along with the depth of the prepared samples at $x = 0$ and $x = 2$ in the composite of In:Ga:Zn = 1:x:1. The EELS data ensure that the oxygen concentration is higher at $x = 2$ than at $x = 0$. This indicates that gallium suppresses the generation of V_O. The oxygen deficiency (vacancy) at the TE/IGZO interface is remarkably increased when $x = 0$. These generated oxygen vacancies are thought to cause BRS, triggering a reduction-oxidation reaction with oxygen ions according to the polarity of the applied voltage.[19]

The nominal device area used for electrical characterization is 100 μm × 100 μm. The BE is grounded while a voltage is applied to the TE. BRS characteristics were noted in the Al/a-IGZO/Al structure. In this work, the examination of BRS is carried out. Fig. 1(b) shows a typical measured current density-voltage (*J-V*) curve with a bipolar voltage sweep in the device with In:Ga:Zn = 1:2:1. An electro-forming process is performed in the voltage range from 0 V to 5 V before the analysis of the RS characteristics without a set compliance current density (CC). The *J-V* curve clearly exhibits hysteresis (a bi-stable state). The HRS and LRS are attributed to the opposite polarity of the applied voltage. A positive voltage results in an HRS, whereas a negative voltage leads to an LRS.

To confirm the modulation effect of the BRS according to the Ga concentration, log-log plots of the *J-V* characteristics were characterized in the devices with In:Ga:Zn = 1:0:1 and In:Ga:Zn = 1:2:1, as shown in Figs. 3(a) and 3(b), respectively. The *J-V* curves positioned toward the right in Figs. 3(a) and 3(b) indicate an electro-forming process from

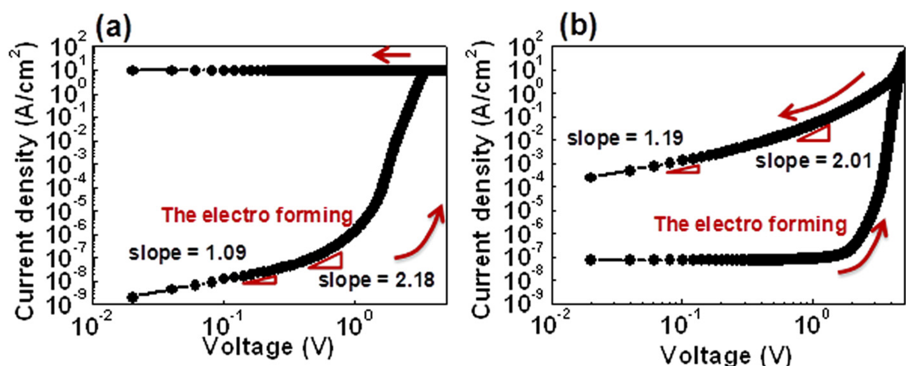

FIG. 3. Measured current density-voltage (*J-V*) characteristics of devices in a double-logarithmic plot in (a) In:Ga:Zn = 1:0:1 and (b) In:Ga:Zn = 1:2:1. Arrows indicate the direction of the voltage sweep. The *J-V* curves positioned toward the right in (a) and (b) indicate the electro-forming process from fresh devices. After the electro-forming process is performed, the *J-V* curves positioned toward the left in (a) and (b) represent a permanent breakdown and a LRS, respectively. The CC is set to 10 A/cm^2 in (a), and the value of the current is not limited in (b).

Downloaded 03 Feb 2013 to 143.248.118.122. Redistribution subject to AIP license or copyright; see http://apl.aip.org/about/rights_and_permissions

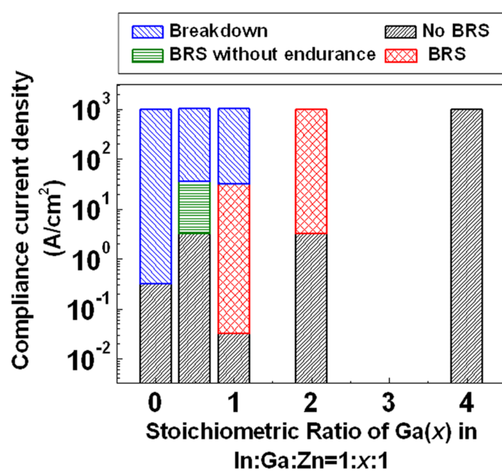

FIG. 4. A graph to show the modulation effects of BRS by controlling the CC with various Ga concentrations. Here, a breakdown means a permanent breakdown. BRS with poor endurance indicates that the devices show BRS with unstable endurance characteristics. No RS indicates that a hysteretic *J-V* curve is not observed.

fresh devices. After an electro-forming process is performed, the *J-V* curves positioned toward the left direction in Figs. 3(a) and 3(b) indicate permanent breakdown and an LRS, respectively. The CC is set to 10 A/cm^2 in Fig. 3(a), and the value of the current density is not limited in Fig. 3(b). Permanent breakdown is observed only at $x=0$ after the electro-forming process. The resistance state of IG$_{x=0}$ZO is altered to a metallic phase, which does not return to a non-metallic state. Figs. 2(a) and 3(a) suggest that this state transition is induced by excessively generated V_O, thus inhibiting a BRS. Fig. 3(b) represents the hysteresis *J-V* curve when $x=2$. In contrast to Fig. 3(a), after the electro-forming process, ohmic conduction ($J \propto V$) in a low-voltage regime and a quadratic term ($J \propto V^2$) in a high-voltage regime were observed in spite of the LRS. In particular, the quadratic voltage dependency arises from the trap-controlled space-charge-limited current (SCLC).[20] It is noteworthy that the trends of the *J-V* curve shown in Fig. 3(b) are very similar to those of the Al/TiO_2/Al-based RRAM.[21,22] It was reported that the BRS of TiO_2 was associated with the oxygen-deficient sites in the top domain of the TiO_2 layer.[20,23] In this experiment, the current-flowing behaviors based on the SCLC in the high-voltage domain indicate that current operations are governed by the variations of the oxygen-deficient region.[24] The BRS is attributed to the reduction-oxidation reaction at the oxygen-deficient IGZO layer.[19] When a positive voltage is applied, O_2^- ions move toward the oxygen-deficient layer. Thus, the oxygen-deficient IGZO layer is thinned down as being oxidized. In other words, as negatively charged oxygen ions fill the oxygen vacancies, the resistance is switched to the HRS during the positive voltage bias. In contrast, O_2^- ions generated by the reduction reaction of IGZO tend to move toward the BE under the negative voltage bias. The BRS from the HRS to the LRS occurs as the oxygen-deficient layer starts to build up.

Figs. 2(a), 2(b), 3(a), and 3(b) show that a properly generated V_O stemming from the chemical reaction of TE/IGZO induces BRS characteristics. In this experiment, it was demonstrated that BRS based on the SCLC is modulated by controlling the V_O concentration through a change in the molar ratio of Ga in the IGZO film.

To clarify the BRS behavior, which is dependent on the V_O concentration, the *J-V* curves are characterized by controlling the CC for various Ga concentrations. As shown in Fig. 4, the BRS characteristics are tunable by changing the stoichiometric ratio (x) and the CC. The CC is controlled from 10^{-2} A/cm^2 to 10^3 A/cm^2. The resistive states are categorized by four groups: (1) breakdown, (2) BRS with poor endurance, (3) BRS, and (4) no BRS. A breakdown indicates a permanent breakdown of the IGZO, which cannot be switched to an HRS. BRS with poor endurance indicates that the value of the resistance fluctuates seriously when the BRS is induced. No BRS indicates that the hysteric *J-V* behavior disappeared. At $x=0$, an excessive V_O is not inhibited by Ga; hence, this inherent and pre-existing V_O leads to the formation of conduction paths. As a result, a permanent breakdown through the aforementioned paths is induced. As noted earlier, the increased gallium concentration (x) contributes to suppressing the generation of V_O.[4] At $x=4$, a high Ga concentration effectively suppresses the generation of V_O; hence, vacant trap densities for electron transport are notably reduced. As a result, the BRS behavior disappears.

To confirm the memory window, i.e., the distinct resistance difference between the HRS and the LRS, a cyclic endurance test was carried out. Figs. 5(a) and 5(b) exhibit the endurance characteristics when In:Ga:Zn = 1:0.5:1 and when In:Ga:Zn = 1:2:1, respectively. It should be noted that significant fluctuation and instability of the HRS arise at $x=0.5$; hence, the resistance interference between the HRS and the LRS becomes problematic. In contrast, reliable endurance is sustained in the range of x from 1 to 2. In other words, a distinctive separation between the HRS and the LRS is consistently sustained in the case of $x=2$. This separation indicates that the reduction-oxidation reaction caused by the

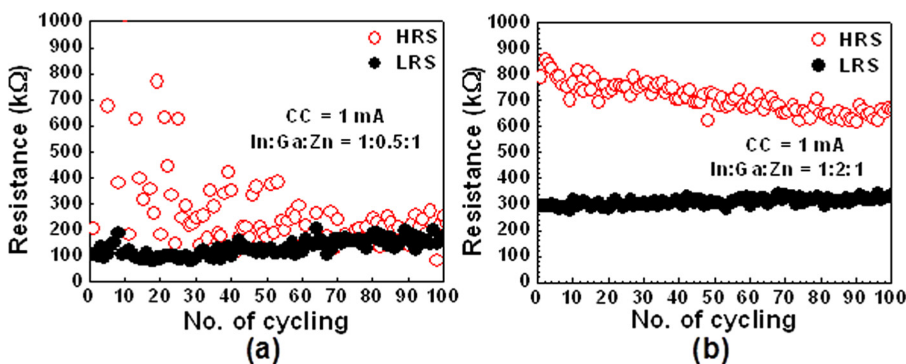

FIG. 5. Endurance characteristics during switching cycling after the electro-forming process for (a) In:Ga:Zn = 1:0.5:1 and (b) In:Ga:Zn = 1:2:1. The CC is set at 10 A/cm^2.

Downloaded 03 Feb 2013 to 143.248.118.122. Redistribution subject to AIP license or copyright; see http://apl.aip.org/about/rights_and_permissions

migration of oxygen ions is controlled according to the polarity of the applied bias, as expected. Therefore, the redox reactions at the oxygen-deficient layer are controllable for high gallium concentrations by the electrical voltage because the generation of V_O is properly suppressed.

The moderately suppressed generation of V_O (when the value of x is approximately 2) enhances the immunity against electrical stress and retains the distinctive separation between the LRS and the HRS under iterative biasing. Although the BRS characteristics look similar for $x = 1$ and $x = 2$, the level of CC is quite different. When $x = 2$, the CC is increased to 10^1 A/cm^2; however, it is 10^{-1} A/cm^2 at $x = 1$. This robustness against current-induced stress is improved when $x = 2$ compared with when $x = 1$. Furthermore, as shown in Fig. 3(b), a BRS in the case of $x = 2$ is actually induced even when the CC is not set. Except $x = 2$, the BRS is inhibited unless a CC is applied during electrical stress. The moderately suppressed oxygen vacancies block off the migration of redundant V_O during a positive voltage bias. The connection of V_O between the BE and the TE leads to the transition to the metallic phase via electrical breakdown.[25] That is, the gallium-rich IGZO layer prevents V_O from being moved back and forth between the BE and the TE. Thus, the optimal value of x is near 2. In conclusion, BRS behavior in gallium-rich IGZO RRAM is tunable by changing the gallium concentration.

In summary, functional RRAM consisting of Al/IGZO/Al was demonstrated here. The stoichiometric ratio (x) was varied from $x = 0$ to $x = 4$ in a composite of In:Ga:Zn = 1:x:1. This ratio controlled the concentration of oxygen vacancies of IGZO, causing the resistive switching properties to be tunable. The increased and reduced oxygen concentrations were analyzed with the aid of EELS. A low gallium concentration (in a range of approximately 0 to 0.5) led to a permanent breakdown or unstable resistive switching, whereas a high gallium concentration (near 4) prohibited the RRAM from exhibiting resistive switching. Therefore, a moderate gallium concentration (ranging from approximately 1 to 2) will allow the RRAM to function properly with a reasonable sensing window and good endurance. These results can provide insight into how to modulate RRAM characteristics comprehensively. Moreover, this investigation can be useful for those who seek to analyze resistive switching characteristics in RRAM devices composed of other materials by adjusting the oxygen concentration.

This work was supported by the Center for Integrated Smart Sensors funded by the Ministry of Education, Science and Technology as a Global Frontier Project (CISS-2011-0031845).

[1]K. Nomura, H. Ohta, A. Takagi, T. Kamiya, M. Hirano, and H. Hosono, Nature (London) **432**, 488 (2004).
[2]T. Iwasaki, N. Itagaki, T. Den, H. Kumomi, K. Nomura, T. Kamiya, and H. Hosono, Appl. Phys. Lett. **90**, 242114 (2007).
[3]G. H. Kim, B. D. Ahn, H. S. Shin, W. H. Jeong, H. J. Kim, and H. J. Kim, Appl. Phys. Lett. **94**, 233501 (2009).
[4]H. Hosono, J. Non-Cryst. Solids **352**, 851 (2006).
[5]J. W. Seo, J.-W. Park, K. S. Lim, J.-H. Yang, and S. J. Kang, Appl. Phys. Lett. **93**, 223505 (2008).
[6]S. Kim and Y. K. Choi, Appl. Phys. Lett. **92**, 223508 (2008).
[7]A. Sawa, Mater. Today **11**, 28 (2008).
[8]R. Waser and M. Aono, Nat. Mater. **6**, 833 (2007).
[9]Y. H. Kim, M. K. Han, J. I. Han, and S. K. Park, IEEE Trans. Electron Devices **57**, 1009 (2010).
[10]T. C. Fung, C. S. Chuang, C. Chen, K. Abe, R. Cottle, M. Townsend, H. Kumomi, and J. Kanicki, J. Appl. Phys. **106**, 084511 (2009).
[11]J. H. Lim, J. H. Shim, J. H. Choi, J. Joo, K. Park, H. Jeon, M. R. Moon, D. Jung, H. Kim, H. Jeon, M. R. Moon, D. Jung, H. Kim, and H.-J. Lee, Appl. Phys. Lett. **95**, 012108 (2009).
[12]M. J. Rozenberg, M. J. Sánchez, R. Weht, C. Acha, F. Gomez-Marlasca, and P. Levy, Phys. Rev. B **81**, 115101 (2010).
[13]C. H. Kim, Y. H. Jang, H. J. Hwang, C. H. Song, Y. S. Yang, and J. H. Cho, Appl. Phys. Lett. **97**, 062109 (2010).
[14]M. Ch. Chen, T. Ch. Chang, Ch. T. Tsai, Sh. Y. Huang, Sh. Ch. Chen, Ch. W. Hu, S. M. Sze, and M. J. Tsai, Appl. Phys. Lett. **96**, 262110 (2010).
[15]Z. Q. Wang, H. Y. Xu, X. H. Li, H. Yu, Y. C. Liu, and X. J. Zhu, Adv. Funct. Mater. **22**, 2759 (2012).
[16]Z. Liao, P. Gao, Y. Meng, H. Zhao, X. Bai, J. Zhang, and D. Chen, Appl. Phys. Lett. **99**, 113506 (2011).
[17]S. J. Seo, J. H. Cho, Y. H. Jang, and C. H. Kim, J. Korean Phys. Soc. **60**, 267 (2012).
[18]T. J. Kim, J. J. Yoon, T. H. Ghong, N. Barange, J. Y. Kim, S. Y. Hwang, Y. D. Kim, S. M. Hwang, J. H. Choi, and J. Joo, J. Korean Phys. Soc. **59**, 3396 (2011).
[19]R. Yang, X. M. Li, W. D. Yu, X. D. Gao, D. S. Shang, X. J. Liu, X. Cao, Q. Wang, and L. D. Chen, Appl. Phys. Lett. **95**, 072105 (2009).
[20]H. Y. Jeong, J. Y. Lee, S.-Y. Choi, and J. W. Kim, Appl. Phys. Lett. **95**, 162108 (2009).
[21]D. B. Strukov, G. S. Snider, D. R. Stewart, and R. S. Williams, Nature (London) **453**, 80 (2008).
[22]Y. Xia, W. He, L. Chen, X. Meng, and Z. Liu, Appl. Phys. Lett. **90**, 022907 (2007).
[23]L.-E. Yu, S. Kim, M.-K. Ryu, S.-Y. Choi, and Y.-K. Choi, IEEE Electron Device Lett. **29**, 331 (2008).
[24]S. Kim, H. Y. Jeong, S.-Y. Choi, and Y.-K. Choi, Appl. Phys. Lett. **97**, 033508 (2010).
[25]D. H. Kwon, K. M. Kim, J. H. Jang, J. M. Jeon, M. H. Lee, G. H. Kim, X. S. Li, G. S. Park, B. Lee, S. Han, M. Kim, and C. S. Hwang, Nat. Nanotechnol. **5**, 148 (2010).

Downloaded 03 Feb 2013 to 143.248.118.122. Redistribution subject to AIP license or copyright; see http://apl.aip.org/about/rights_and_permissions